MASTER

THERMOHYDRAULIC AND THERMAL STRESS ASPECTS OF A POROUS BLOCKAGE IN AN LMFBR FUEL ASSEMBLY

by

Tuncer M. Kuzay, William W. Marr, H. W. Helenberg,
Teoman Ariman, Richard E. Wilson, and Dean R. Pedersen

Prepared for
5th SMiRT Conference
Berlin, Germany
August 13-17, 1979

U of C-AUA-USDOE

ARGONNE NATIONAL LABORATORY, ARGONNE, ILLINOIS

Operated under Contract W-31-109-Eng-38 for the
U. S. DEPARTMENT OF ENERGY

MASTER

Abstract

The current safety scenarios of Liquid Metal Fast Breeder Reactors (LMFBR) under local fault propagation include the study of a hypothetical accident initiated by the formation of an external debris porous blockage in a fuel subassembly.

In this preliminary experimental and analytical investigation, a non-heat-generating porous blockage was postulated to cover 18 flow channels of a 37 pin Fast Test Reactor (FTR) type fuel subassembly. The axial extent of the blockage is 50 mm. The blockage material is stainless steel (SS 316) with 30 percent average porosity (percent void volume).

The blockage and the pins were modeled with a finite element technique and the thermal field in the blockage was predicted. This thermal field was utilized to do a planar thermal stress analysis of the postulated blockage.

To verify the analytical model and also to better understand the thermal-hydraulics of such a porous blockage out-of-pile tests were conducted in a sodium loop. Data from the out-of-pile tests was utilized to calibrate and improve the analytical model.

1. Introduction

The current safety scenarios of liquid metal fast breeder reactors (LMFBR) under the local fault propagation include hypothetical accidents initiated by the formation of a blockage around the fuel pins in a given fuel subassembly. Thermohydraulic phenomena in the subassembly upon formation of a hypothetical planar blockage have been the subject of many experimental and theoretical studies to date [1 to 6].

More recently, however, the matter of the hypothetical formation of non-planar blockages in subassemblies has been brought into the safety arguments [7 to 10]. Such blockages can be heat-generating or non-heat-generating depending on the assumptions regarding the source of the hypothesized particulate debris. The porosity is determined by the size and the shape of the particulate matter. The radial and axial extent of the postulated blockage is determined largely by pragmatic arguments on failure and/or detectibility [8 to 10]. Presently, a 50 mm long porous blockage covering flow channels around a basic seven-pin cluster in a 37-pin test bundle [11] has been favored in the experiments. A variation of such a postulated blockage which covers 18 flow channels in a 37-pin Fast Test Reactor (FTR) type subassembly is shown in Figure 1. The particular configuration of the blockage was chosen to assure a planned pin failure in a proposed Sodium Loop Safety Facility (SLSF) in-pile experiment [16].

Unlike the case of the planar blockages, thermohydraulic and thermal stress aspects of such 3D porous blockages are not well understood to assure successful in-pile tests. First, the porous nature of the sintered steel (SS 316) model blockage introduces uncertainties in the mechanical and physical properties for pretest calculations. Second, non-boiling and boiling heat transfer in such thick porous media immersed in a sodium stream is virtually unknown except for the not-so-relevant case of sintered wick heat pipes. In the present case, the heat is applied to the blockage internally by the pins (Figure 1) as discreet cylindrical heat flux sources. Third, as it is intuitively expected that rather large thermal gradients will be induced within the blockage both radially and axially, thermal stresses need to be assessed so as not to cause a premature failure of the blockage jeopardizing objectives of any prospective in-pile LMFBR safety test.

In order to find answers to some of these questions analytical and experimental efforts have been undertaken and this paper reports the preliminary results from these efforts.

2. The Blockage and the Test Section Geometry

The model blockage is shown in Figure 1. It is made of sintered stainless steel with approximately 60 μm spherical particles with a measured average porosity of $\varepsilon = 30 \mp 2$ percent. The blockage is 50 mm long. It is machined to accommodate 16 nominal size FTR type pins of 5.84 mm diameter with + 0.0254 mm clearance tolerance at room temperature so that when it is heated to about 810 K temperature (the expected average operational temperature in the reactor) the clearance closes up and no sodium leakage between the pins and the blockage can occur. The inner four pins are completely surrounded by the blockage whereas the peripheral three pins have only 2/3 of their perimeter covered by the blockage with the remaining nine are 2/3 exposed to the flowing sodium (Figure 2a).

The inner seven pins were heated electrically. The peripheral nine pins were dummy pins. The heated pins had a 305 mm long heated length at a maximum rate of 10 kW per pin. Each pin had four chromel-alumel thermocouples grounded to the inside of 0.38 mm thick stainless steel clad. Two of these thermocouples could be located within the blockage zone with the remaining two located upstream and downstream of the blockage. Additional thermocouples were located strategically external to the pins in the test section to measure upstream, downstream (wake) and the bulk temperature of the coolant sodium along the sides of the blockage.

The test section was made of a 50.8 mm nominal tube with 50.4 mm ID. Three threaded stainless steel rods with the same diameter as the heated and dummy pins held the blockage - pin assembly together using three clamped templates far removed from the blockage region. Additional thermocouples, pressure sensors, two electromagnetic flowmeters and nine external accelerometers (to detect boiling in future tests) comprised the rest of the test section instrumentation. This test section was connected to an existing sodium test loop. The test section plenum was filled with argon gas which could be regulated to provide any desired pressure.

3. Out-of-Pile Tests

Out-of-pile tests were planned to run in two stages. The first stage consisted of checkout runs and non-boiling low power tests. Once the operation of the loop and the heat transfer within the blockage are well understood the second stage of boiling tests will be conducted. To date, only the first stage has been completed and only some preliminary results are available.

The low power tests were run with 1.6 KW/m to 7.0 kW/m pin power at sodium flow rates ranging from 570 Kg/hr to 1900 Kg/hr in the test section.

In Figure 2, typical data obtained by thermocouples in and around the blockage are shown. The Figure 2a depicts schematically a top view of the disposition of the thermocouples within the blockage. The thermocouples are shown with different symbols so that they can be identified in Figure 2b, which is a side view. From these figures one can see that the center plane of the blockage contains three pairs of pin thermocouples. One other pair is located 19 mm below the center plane and three other pairs respectively at 13 mm, 19 mm and 22 mm above the center plane. Two thermocouples measured upstream and downstream flow temperature close to the side surface and three others were located in the wake region with a pair of these only 1.6 mm away from the downstream face and the remaining one 25 mm away from it.

Comparison between the measured and the predicted temperatures within the porous blockage will be discussed in a later section following a description of the analytical model.

4. Analytical Model

The blockage and the heater pins were modelled using a conventional finite element code with an automatic node generation capability [12]. The blockage has 6-fold symmetry and the model simulates one sixth wedge of the blockage as illustrated in Figure 2a. A detailed version of the same wedge is shown in Figure 3. The constant heat flux is applied to the inside of the clad in the central seven heater pins. The two dummy pins within the wedge in Figure 3 are represented, respectively by the lower pin and the indicated adiabatic boundary to the right of it. The upstream face of the blockage is subject to impingement heat transfer whereas the downstream face is cooled by a recirculating wake flow [13]. The rest of the model surfaces are assumed adiabatic except those surfaces swept by the sodium flow. The blockage is represented by five axial segments resulting in a 260-node model. Internal to the porous blockage only conductive heat transfer is allowed. The thermal conductivity of the sodium saturation sintered steel blockage is computed by

$$k_b = k_{st}\left[1 + \frac{\varepsilon\ (k_s - k_{st})}{(1 - \varepsilon^{0.33})\ k_s + \varepsilon^{0.33}\ k_{st}}\right]$$

Here, k_{st} and k_s are the temperature dependent thermal conductivities for steel and sodium respectively. All thermal properties for materials in the blockage assembly are temperature dependent. The coolant temperatures at the upstream and the downstream faces of the blockage were obtained from the experimental measurements.

5. Comparison of Predicted and Measured Temperatures

The analytically predicted temperature field in the mid-plane of the blockage corresponding to the experimental case of Figure 2 is depicted in Figure 4. This sample case is typical of all the results obtained so far for various flow-power-inlet temperature combination. In this particular case, the flow is 1900 Kg/hr, pin power is 7.0 KW/m and the inlet sodium temperature is 706 K. The predicted temperature of 981 K for the center pin differs from data by about 10 K. The two thermocouples in the next pin which are also embedded in the blockage indicated respectively 966 K and 595 K compared to the computed temperature 964 K for the former and 865 K (average value between the two large nodes in the model) for the latter. The other two thermocouples in the remaining heater pin read 952 K and 937 K respectively. Again averaging the two nodes we obtain a predicted temperature of 918 K. From these comparisons one can conclude that although the agreement between the data and predictions is reasonably good, overall the radial temperature gradient in the center plane is somewhat overestimated by the model. It should also be noted that the maximum temperatures in the blockage should occur downstream of the center plane. This is due to thermal axial asymmetry in the blockage largely because of the existence of a warmer wake region compared to a cooler stagnation region at the upstream face. Secondly, the axial convective heat transfer on the sides of the blockage also contributes to this phenomenon. The model indicated this rather well. The axial nodes above the center plane for the central region of the blockage are at somewhat higher temperatures.

It is also expected that temperatures at the central region of the blockage should not be very sensitive to the magnitude of the convective heat transfer assumed at the ends of the blockage. The core temperatures are somewhat more sensitive to the sidewall heat transfer coefficient since the blockage has an aspect ratio of L/D ~2. A 50 percent increase in the sidewall convective heat transfer coefficient reduces core region temperatures by ~8 to 10 K. A decrease of the model blockage length from 50 mm to 40 mm has no affect on the computed center plane temperatures.

The success of the analytical model is best tested by a comparison of the measured axial temperature gradients against the predicted ones. The magnitude of the axial temperature gradient relative to the radial gradient is also important in justifying the use of a plane strain assumption in the calculation of the thermal stresses. From the limited data available it seems that the upper half of the blockage has relatively flat axial temperature profiles. Much greater axial temperature gradients exist in the lower half of the blockage. This is in good agreement with the predictions.

Prediction of the pin power level to produce boiling in the blockage is another objective of the tests. This power level is regarded as a "failure threshold" since continued increase in the power level beyond the threshold will presumably initiate pin failures. In the non-boiling tests, the pin power level was gradually increased in steps of 0.5 kW for preset thermal hydraulic test conditions. The temperature rise in the center pin (hottest element) corresponding to the power step was extrapolated to predict the power level where boiling in the blockage could occur. Extrapolation of the experimental data yielded a pin power of 11.40 kW/m which is within 10 percent of the analytically predicted value of 12.78 kW/m. These will be verified by future boiling tests.

6. Thermal Stresses

An assessment of the thermal stresses in the blockage is needed to prevent a premature failure of the sintered steel blockage in the in-pile or out-of-pile safety tests. An earlier analytical simulation [14] without the benefit of the present out-of-pile test data to "fine-tune" the analytical model resulted in the temperature distribution as shown in Figure 5. The temperatures are for a cross-section slightly above the center plane of the blockage where the maximum temperatures were predicted to occur at the time of the sodium boiling in the blockage under FTR conditions.

This above temperature field was used to do a thermal stress analysis on the model blockage. For this purpose a modified version of the finite element computer code [illegible]-PLAST [15] was used. This model consists of 177 triangular elements and 132 nodes. Plane strain was assumed and the porous blockage material was treated as a continuum. The model and the computed stress field corresponding to the temperature distribution in Figure 5 is shown in Figure 6. To maintain clarity in the figure, the stress distribution is represented by shaded areas. The location of calculated maximum stress is in between the outer heater pins. Currently available limited test data on 30 percent porous, SS 316 sintered material reveals that the yield stress is highly temperature dependent and representative values are as follows: 68.9 MPa at 311 K and 11.7 to 12.4 MPa at 1366 K. In view of this information it is clear from Figure 6 that, the planar thermal stresses induced in the porous blockage are below the yield stress at the corresponding temperature and therefore the thermal stresses will not cause premature failure of the blockage. Failure of the blockage will occur, however, through melting of the pin cladding and possible fuel release at elevated power levels.

7. Conclusions

Several conclusions have been drawn from the current state of the out-of-pile blockage tests and the analytical predictions:

The radial temperature gradients in the blockage are somewhat smaller than those predicted. The upper half of the blockage exhibits substantially more uniform axial temperature profiles. The lower half of the blockage is, however subjected to significant axial temperature gradients. With the benefit of experimental data obtained from the sodium cooled seven heater pin out-of-pile porous blockage tests, a previous analytical model has been "calibrated" to bring the predicted in-blockage temperatures in substantial agreement with those observed in the tests.

Acknowledgements

This work is conducted under the auspices of U.S. DOE. Careful typing by Terri Ashford is appreciated.

References

[1] HAN, J. T. and FONTANA, M. H., "Blockages in LMFBR Fuel Assemblies", Thermal and Hydraulic Aspects of Nuclear Reactor Safety, Vol. 2, LMFBR, ASME, N.Y., N.Y., 1977.

[2] KIRSCH, D., "Investigation on the Flow and Temperature Distribution Downstream of Local Coolant Blockages in Rod Bundle Subassemblies", Nuclear Engineering and Design, 31, pp. 266-79 (1974).

[3] BROOK, A. J., HUBER, F., and PEPPLER, W., "Temperature Distribution and Local Boiling Behind a Central Blockage in a Simulated FBR-Subassembly", Proc. of Int. Meeting on Fast Reactor Safety and Related Physics, October 5-8, 1967, Chicago, IL

[4] DEVRIES, J. F., HOEVE, J. C., and DORR, B., "Local Boiling in a Test Bundle Simulating a Sixth Part of an LMFBR Subassembly Having a Large Flat Type Central Flow Blockage", ECN-77-137, September 1977.

[5] HERBERT, R., KIRSCH, D., "A Comparison of Temperature Distributions Calculated by the SABRE Program with Experimental Results", KFK 2205, AEEW-R 987, July 1975.

[6] DOMANUS, H. M., and SHA, W. T., "Numerical Results for a Hexagonal Fuel Assembly With a Planar Blockage Using the COMMIX-1A Computer Code", NUREG/CR-0489, also ANL-CT-79-8, September 1978.

[7] FAUSKE, H. K., GROLMES, M. A., and CHAN, S. H., "An Assessment of Fuel Failure Propagation in LMFBRs", Proc. of Int. Meeting on Fast Reactor Safety, and Related Physics, October 5-8, 1976, Chicago, IL

[8] SCHULTHEISS, G. F., "Analysis of the Formation of Local Coolant Blockages in Sodium Cooled Fast Breeder Reactors", EURFNR-1394 (also KFK 2331).

[9] SCHULTHEISS, G. F., "Model for Formation and Growth of Local Blockages in Grid Spaced Fast Sodium Cooled Breeder Fuel Elements", Nuclear Engineering and Design 43, pp. 329-41 (1977).

[10] SMIDT, D., and SCHLEISIEK, K., "Fast Breeder Safety Against Propagation of Local Failures", Nuclear Engineering and Design, 40, pp. 393-402 (1977).

[11] KRAMER, W., et. al., "Coolant Blockage Experiments in BR-2 (Mol 7C)", KFK 1274/4, pp. 123-125, May 1975.

[12] RAGLAND, W. A., and NELSON, J. E., ANL-RDP-73, p. 65, July 1978.

[13] VIRK, P. S., "Heat Transfer from the Rear of a Cylinder in Transverse Flow", Trans. ASME, Ser. C, 92-1, 206 (1970).

[14] KUZAY, T. M., ANL-RDP-74, p. 6.9-6.10, April 1978.

[15] WANG, C. Y., and SZAWADZKI, "A User's Manual for Finite-Element Computer Code CREEP-PLAST", ANL-CT-78-21, January 1978.

[16] WARINNER, D. K., ANL-RDP-72, pp. 6.3-6.7, June 1978.

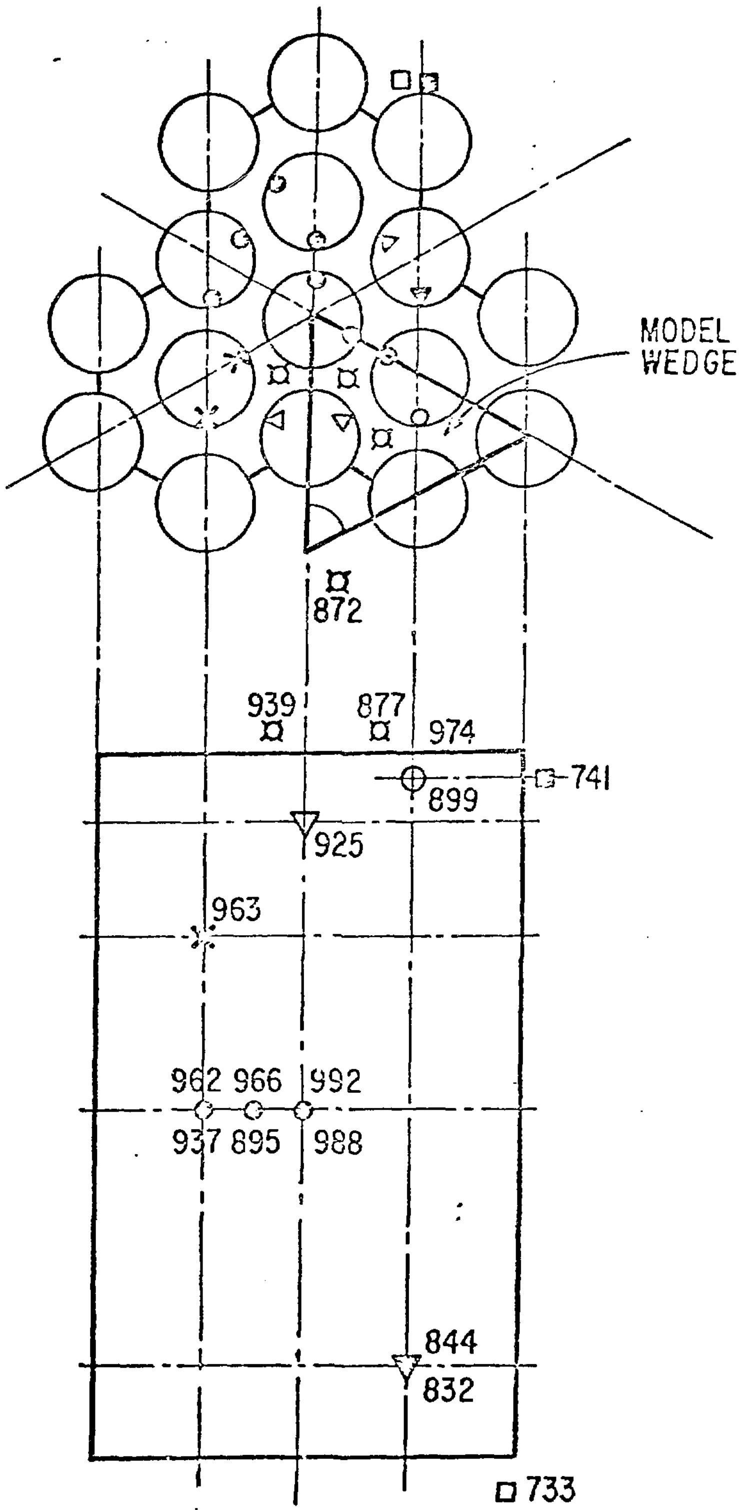

MODEL
WEDGE
872
939
877
974
741
899
925
963
962 966 992
937 895 988
844
832
733

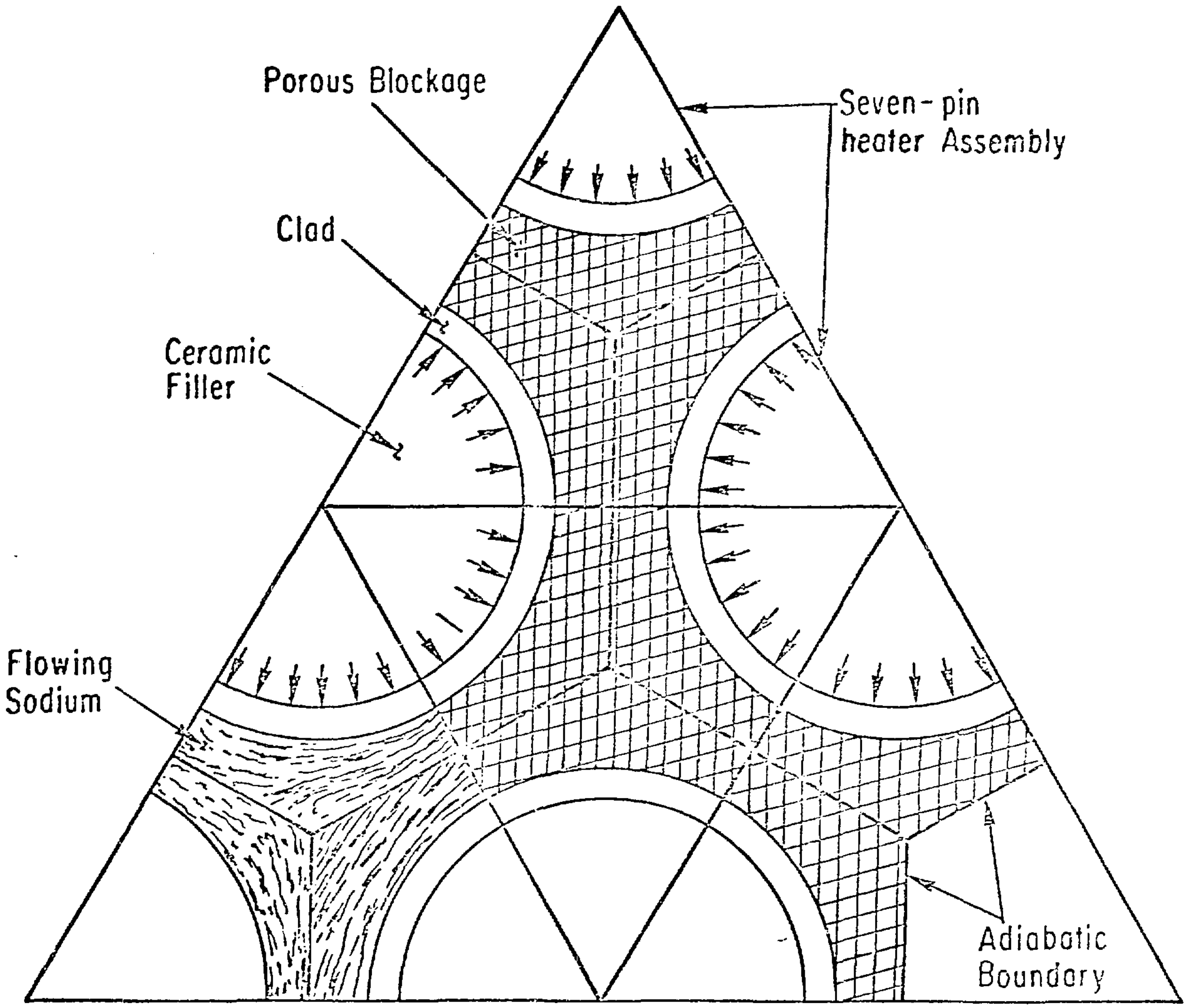

Porous Blockage
Seven-pin heater Assembly
Clad
Ceramic Filler
Flowing Sodium
Adiabatic Boundary

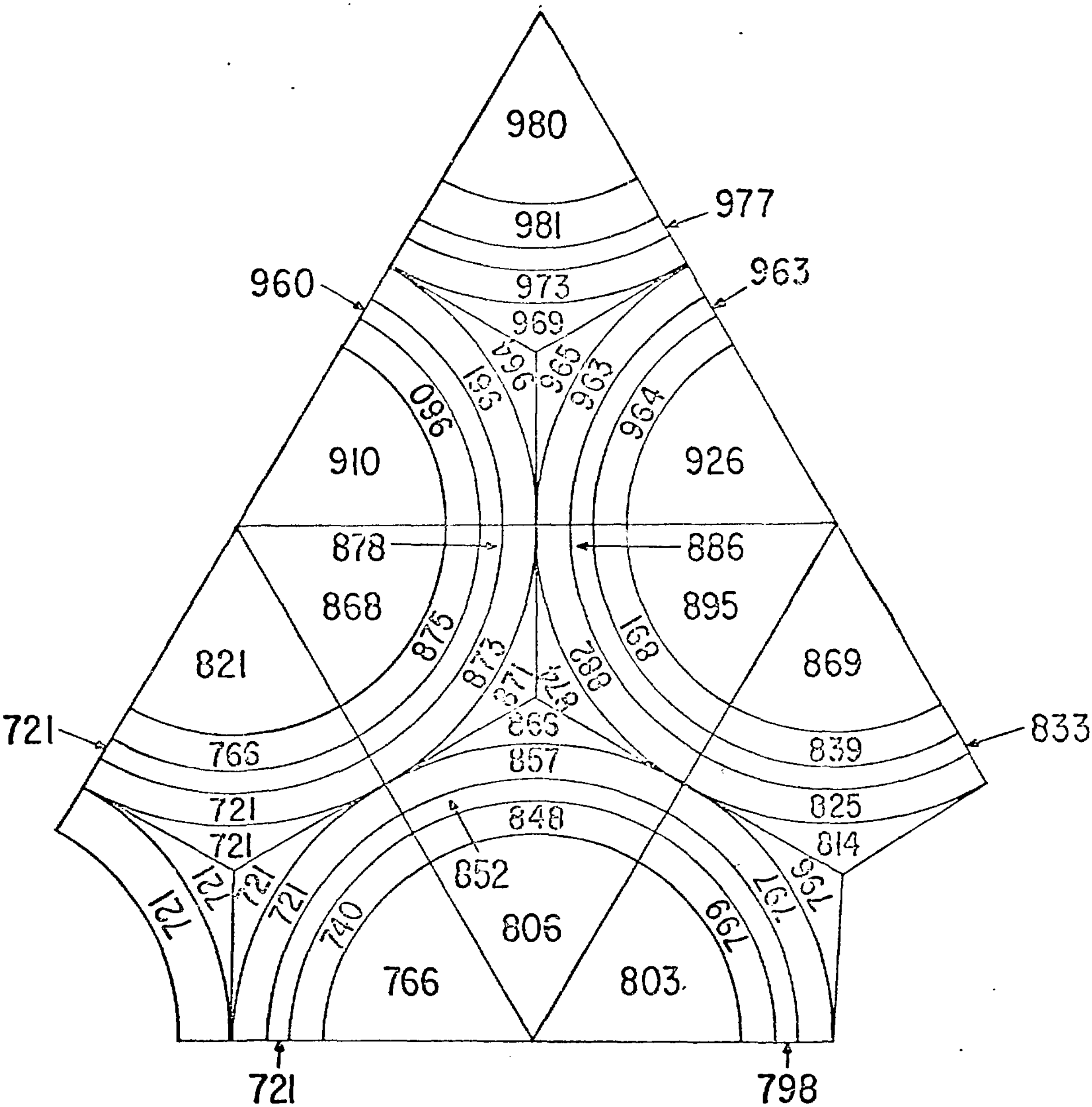
980
981
977
960
973
963
969
964
965
961
963
960
964
910
926
878
886
868
895
875
891
821
869
873
882
871
874
865
721
833
766
857
839
721
825
848
721
814
721
721
721
852
797
796
721
740
806
799
766
803
721
798

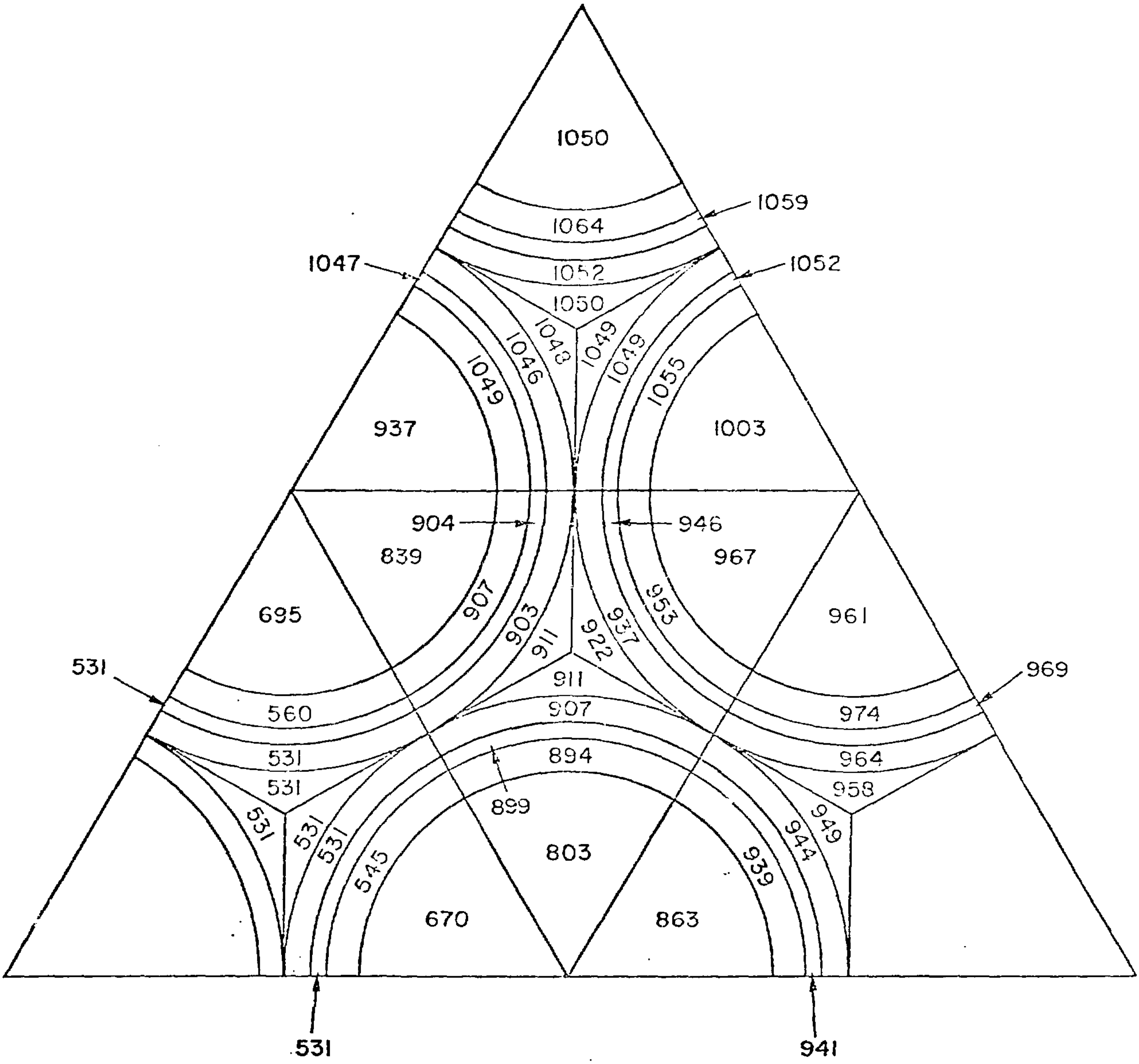
1050
1059
1064
1047
1052
1052
1050
1046
1048
1049
1049
1049
1055
937
1003
904
946
839
967
695
907
903
911
922
937
953
961
531
969
911
907
560
974
531
894
964
531
958
531
531
531
899
949
944
545
803
939
670
863
531
941

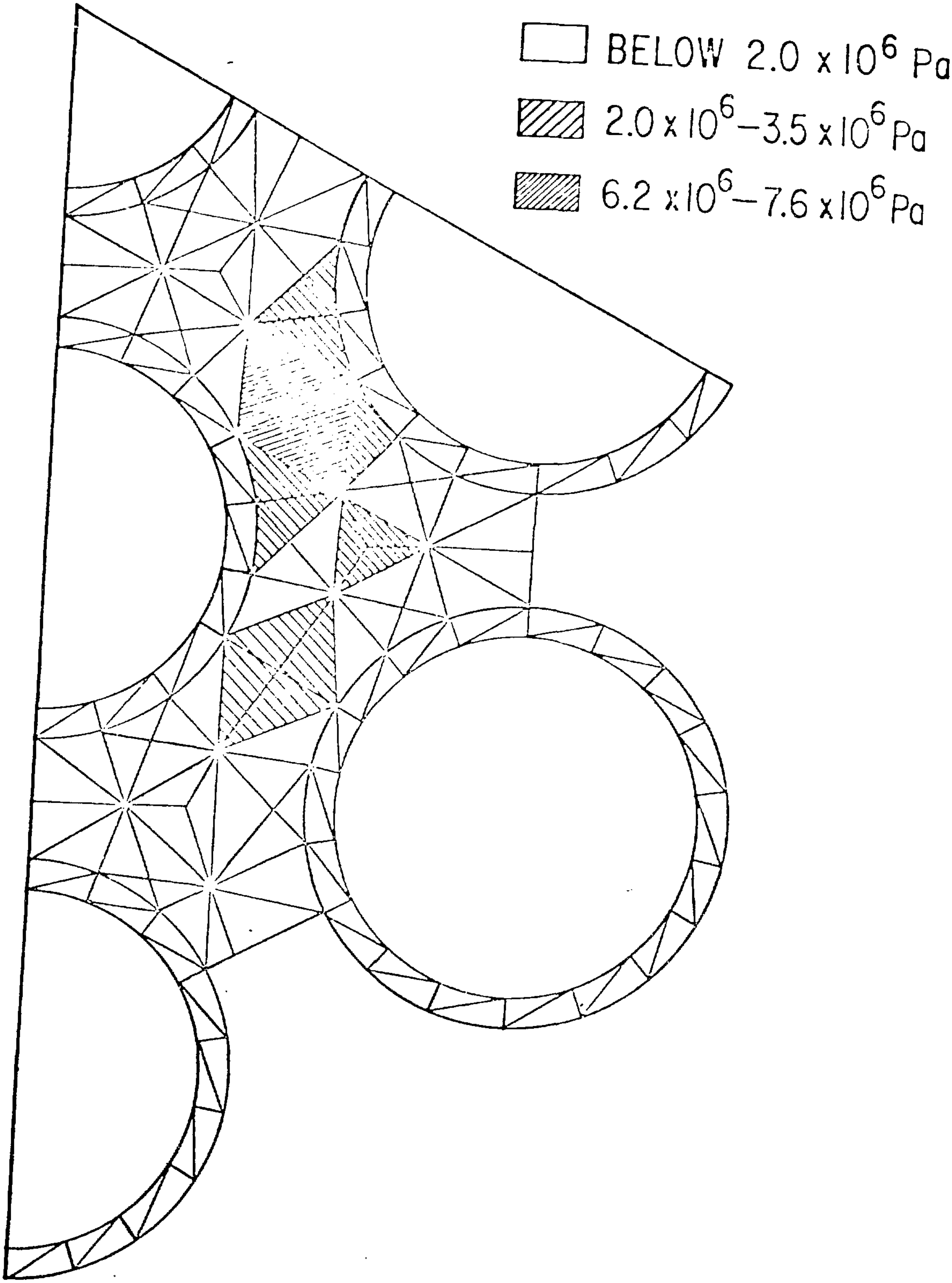

BELOW 2.0 x 10^6 Pa
2.0 x 10^6 – 3.5 x 10^6 Pa
6.2 x 10^6 – 7.6 x 10^6 Pa

Figure Titles

Figure 1. Geometry of the 7-heater pin sintered steel porous blockage (ϵ = 0.39).

Figure 2. Top view of blockage showing the thermocouple locations and the 1/6th wedge of the analytical model.

Figure 2b Side view of the blockage cylinder showing elevations of the thermocouples and data for the sample test (K) - not to scale.

Figure 3. Analytical model for the 7-heater pin blockage, 1/6th wedge.

Figure 4. Analytically predicted node temperatures in the center plane of the blockage (K).

Figure 5. An earlier model prediction of temperatures at the time of sodium boiling in the blockage next to the center pin (°C).

Figure 6. Finite element stress model and the predicted stress distribution.